*Int. J. Solids Structures* Vol. 22, No. 8, pp. 845–857, 1986
Printed in Great Britain.

0020-7683/86 $3.00 + .00
Pergamon Journals Ltd.

# DYNAMIC STRESS INTENSITY FACTORS FOR BURIED PLANAR AND NONPLANAR CRACKS

A. H. SHAH and K. C. WONG
Department of Civil Engineering, University of Manitoba, Winnipeg, Canada R3T 2N2

and

S. K. DATTA
Department of Mechanical Engineering and Co-operative Institute for Research in Environmental Sciences, University of Colorado, Boulder, CO 80309, U.S.A.

(*Received* 4 *August* 1985)

**Abstract**—The scattering of time-harmonic plane longitudinal, shear and Rayleigh waves by a crack in two dimensions embedded in a semi-infinite homogeneous isotropic elastic half-space has been studied in this paper. Two problems have been considered: a straight crack and a Y-shaped crack. A hybrid numerical technique combining a multipolar representation of the scattered field in the half-space with the finite element method has been used to obtain the stress-intensity factors for the crack tips. Numerical results for the various crack geometries and the incident waves are discussed in this paper.

## 1. INTRODUCTION

Problems of scattering of elastic body and surface waves by a crack near a surface are of considerable current interest for ultrasonic nondestructive evaluation. In recent years Achenbach and his co-workers[1–9] have used an integral equation approach to study scattering by surface-breaking and subsurface planar cracks. They have also developed a ray theoretic technique to analyze scattering by planar cracks[10–14]. In a recent article[15] Visscher uses a boundary integral equation formulation for scattering by planar cracks in a half-space. He gives detailed numerical results for scattering of SH waves. Scattering of SH waves by surface-breaking planar cracks were studied by Stone *et al.*[16] using an integral equation formulation and by Datta and co-workers[17–19] using a matched asymptotic expansion technique valid at long wavelengths as well as by a hybrid combined finite element and analytical expansion technique, which is useful for long and intermediate wavelengths.

The hybrid technique used in [17–19] has the advantage that it can be used for any arbitrarily shaped scatterers as well as for more than one scatterer. Recently, it has also been used to study scattering of SH waves by a normal and arbitrarily oriented planar crack in a thick plate[20–22].

In this paper two-dimensional elastic wave scattering by a crack lying in a semi-infinite linearly elastic isotropic homogeneous medium has been studied. Two types of cracks have been considered: a straight crack and a Y-shaped crack. The results for the former case have been found to agree with those obtained in [4–7] for vertical and horizontal straight cracks. We also present results for oblique straight cracks with angles of inclination not considered in [9]. Thus these results complement those of [9]. Finally, we present results for a Y-shaped crack which are new and are found to differ considerably from those for a straight crack.

## 2. FORMULATION AND SOLUTION

For the case of plane-strain, an analytical procedure was presented in [23] for a circular cylindrical pipe embedded in a semi-infinite medium. Also, a hybrid combined analytical and numerical method was presented[24] when irregularly shaped objects are embedded in an infinite medium. Here we modify and extend the hybrid modeling to the case of irregularly

shaped objects embedded in a semi-infinite medium. The same technique was recently used to analyze surface displacements due to subsurface cavities[25].

As shown in Fig. 1 interior region $R_2$, bounded by a circular boundary $B$ of radius $R_B$, contains all the scattering inhomogeneities (e.g. cracks) and anisotropy. The exterior host region $R_1$ is assumed to be isotropic and homogeneous having Lamé constants $\lambda$ and $\mu$ and mass density $\rho$. The displacement associated with the plane incident waves are denoted by $u^{(i)}(x, y, t)$, and it will be assumed that their directions of propagation make an angle $\gamma$ with the negative $y$-axis. Only harmonic time dependence of the form $e^{-i\omega t}$, where $\omega$ is the circular frequency, will be considered.

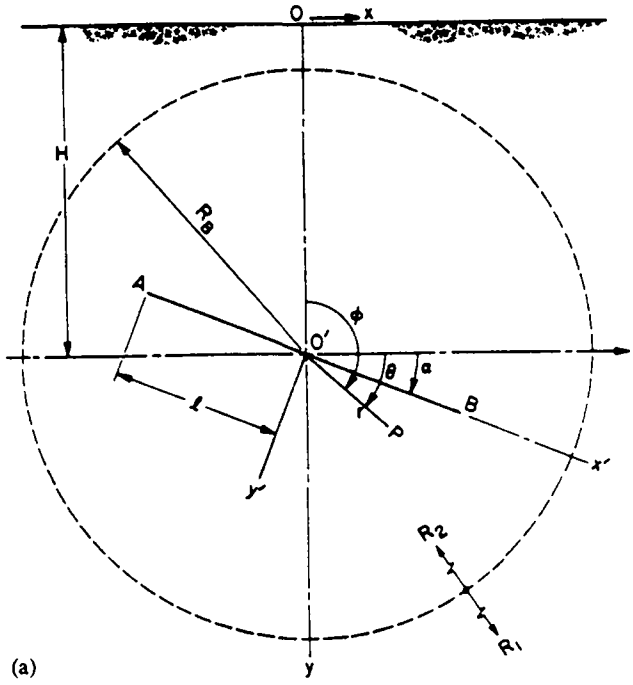


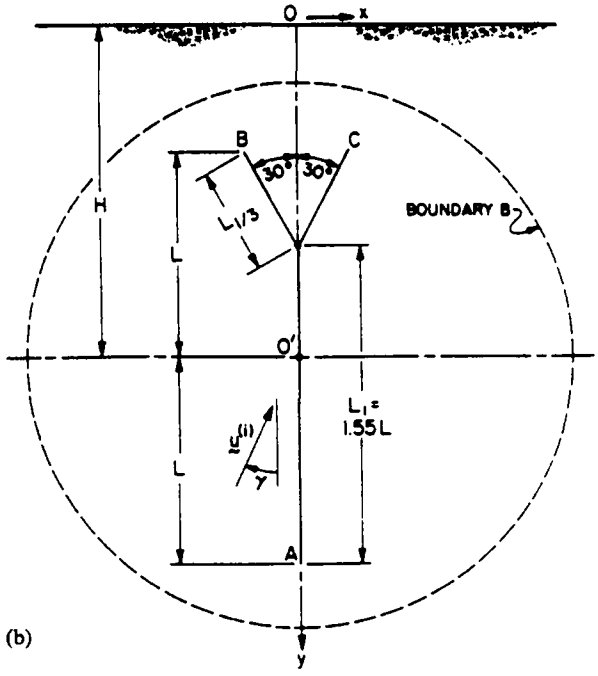


Fig. 1. Geometry of (a) the straight crack and (b) the branched (Y) crack.

Subdividing $R_2$ into finite elements having $N_I+N_B$ number of nodes, $N_I$ being the number of interior nodes and $N_B$ the number of boundary nodes, the energy functional, $F$, can be written as

$$F = \mathbf{q}_{x_I}^{*T} S_{II} q_{x_I} + \mathbf{q}_{x_I}^{*T} S_{IB} \mathbf{q}_{x_B} + \mathbf{q}_{x_B}^{*T} S_{IB}^{T} \mathbf{q}_{x_I} + \mathbf{q}_{x_B}^{*T} S_{BB} \mathbf{q}_{x_B}, \tag{1}$$

in which $\mathbf{q}_{x_I} = \mathbf{q}_{x_I}^{(2)}$, $\mathbf{q}_{x_B} = \mathbf{q}_{x_B}^{(2)}$, the superscripts $*$ and $T$ designate complex conjugate and transpose, respectively. The nodal displacements $\mathbf{q}_{x_j}^{e}$ have two components $u_{x_j}$ and $u_{y_j}$ along the $x$ and $y$ directions, respectively. The element impedance matrices $S_{ij}$ are defined as

$$[S^e] = \int_{R_e} \int ([B^e]^T [D] [B^e] - \rho_e \omega^2 [L]^T [L])\, \mathrm{d}x\, \mathrm{d}y, \tag{2}$$

in which

$$[B^e] = \begin{bmatrix} \dfrac{\partial}{\partial x} & 0 \\ 0 & \dfrac{\partial}{\partial y} \\ \dfrac{\partial}{\partial y} & \dfrac{\partial}{\partial x} \end{bmatrix} \begin{bmatrix} L_1 & 0 & L_2 & 0 & \cdots \\ 0 & L_1 & 0 & L_2 & \cdots \end{bmatrix} = [N][L],$$

where $L_j(x, y)$ are shape functions. For isotropic material, $[D]$ is given by

$$[D] = \begin{bmatrix} \lambda_e + 2\mu_e & \lambda_e & 0 \\ \lambda & \lambda_e + 2\mu_e & 0 \\ 0 & 0 & \mu_e \end{bmatrix}.$$

In the exterior region $R_1$ the free field displacements ($u_r^{(0)}$, $u_\theta^{(0)}$) and the scattered displacements ($u_r^{(s)}$, $u_\theta^{(s)}$) can be written as

$$u_r^{(0)} = \sum_{n=-\infty}^{\infty} \left[ C_n G_{r_1}^{(n)} + D_n G_{r_2}^{(n)} \right] \mathrm{e}^{in\phi}, \tag{3}$$

$$U_\theta^{(0)} = \sum_{n=-\infty}^{\infty} \left[ C_n G_{t_1}^{(n)} + D_n G_{t_2}^{(n)} \right] \mathrm{e}^{in\phi},$$

$$\begin{aligned} u_r^{(s)} = \sum_{n=-N_1}^{N_2} \Bigg[ & a_{n_1} \left\{ D_{r_1}^{(n)} \mathrm{e}^{in\phi} + \sum_{m=-M_1}^{M_2} (P_{mn} G_{r_1}^{(m)} + Q_{mn} G_{r_2}^{(m)}) \mathrm{e}^{im\phi} \right\} \\ & + a_{n_1+N_B} \left\{ D_{r_2}^{(n)} \mathrm{e}^{in\phi} + \sum_{m=-M_1}^{M_2} (R_{mn} G_{r_1}^{(m)} + S_{mn} G_{r_2}^{(m)}) \mathrm{e}^{im\phi} \right\} \Bigg] \end{aligned} \tag{4}$$

$$\begin{aligned} u_\theta^{(s)} = \sum_{n=-N_1}^{N_2} \Bigg[ & a_{n_1} \left\{ D_{t_1}^{(n)} \mathrm{e}^{in\phi} + \sum_{m=-M_1}^{M_2} (P_{mn} G_{t_1}^{(m)} + Q_{mn} G_{t_2}^{(m)}) \mathrm{e}^{im\phi} \right\} + a_{n_1} \\ & + a_{n_1+N_B} \left\{ D_{t_2}^{(n)} \mathrm{e}^{in\phi} + \sum_{m=-M_1}^{M_2} (R_{mn} G_{t_1}^{(m)} + S_{mn} G_{t_2}^{(m)}) \mathrm{e}^{im\phi} \right\} \Bigg], \end{aligned}$$

where $N_2 = M_2 = \frac{1}{2}N_B$, $N_1 = M_1 = N_2 - 1$, and $n_1 = n + N_2$. $C_n$, $D_n$ are constants depending on the characteristic of the wave (P, SV or Rayleigh) and location of the source. The

expressions for constants $C_n$, $D_n$ and the functions $G_{r_j}^{(n)}$, $G_{i_j}^{(n)}$, $D_{r_j}^{(n)}$ and $D_{i_j}^{(n)}$ are given in [23–25] and those for $P_{mn}$, $Q_{mn}$, $R_{mn}$ and $S_{mn}$ can be found in [26, 27].

Evaluating eqn (4) at each of the $N_B$ points on the circular boundary $B$, the scattered displacement vector $\mathbf{q}_{r_B}$ can be written as

$$\{\mathbf{q}_{r_B}^{(s)}\} = [G_{r\theta}]\{a\} \tag{5}$$

or

$$\{\mathbf{q}_{r_B}^{(s)}\} = [G_{xy}]\{a\}, \tag{6}$$

where

$$[G_{xy}] = [T]^T[G_{r\theta}],$$
$$\mathbf{q}_{r_{B_j}}^{(s)} = \{u_{r_{B_j}}^{(s)}, u_{\theta_{B_j}}^{(s)}\}^T, \qquad \mathbf{q}_{x_{B_j}}^{(s)} = \{u_{x_{B_j}}^{(s)}, u_{y_{B_j}}^{(s)}\}^T,$$

and the components $T_i$ of the transformation matrix are

$$[T_i] = \begin{bmatrix} \cos\theta_i & \sin\theta_i \\ -\sin\theta_i & \cos\theta_i \end{bmatrix}.$$

Using the stress–strain and strain–displacement relations, the nodal scattered stress vector can be written from eqns (4) and (5) as

$$\{\boldsymbol{\sigma}_{r_B}^{(s)}\} = [F_{r\theta}]\{a\} = [F_{r\theta}][G_{r\theta}]^{-1}\{\mathbf{q}_{r_B}^{(s)}\}, \tag{7}$$

where

$$\boldsymbol{\sigma}_{r_{B_j}}^{(s)} = \{\sigma_{rr_{B_j}}^{(s)}, \sigma_{r\theta_{B_j}}^{(s)}\}^T.$$

From eqn (7) it can be seen that if the final equations are to be solved in terms of the nodal displacements the complex matrix $[G_{r\theta}]$ has to be inverted as reported in [24]. Here we present an alternate approach where the equations are solved in terms of the generalized coordinates $\{a\}$, thus avoiding the inverse. To this end we write the expression for the virtual work done on the boundary $B$ as

$$\delta\pi = \int_B \{\delta q_{r_B}^{*(1)}\}^T\{\boldsymbol{\sigma}_{r_B}^{(1)}\}\, \mathrm{d}\gamma, \tag{8}$$

in which

$$\mathbf{q}_{r_B}^{(1)} = \mathbf{q}_{r_B}^{(s)} + \mathbf{q}_{r_B}^{(0)},$$
$$\boldsymbol{\sigma}_{r_B}^{(1)} = \boldsymbol{\sigma}_{r_B}^{(s)} + \boldsymbol{\sigma}_{r_B}^{(0)},$$

where $\mathbf{q}_{r_B}^{(0)}$ and $\boldsymbol{\sigma}_{r_B}^{(0)}$ are free-field quantities. Noting $\delta\mathbf{q}_{r_B}^{(1)} = \delta\mathbf{q}_{r_B}^{(s)}$ and substituting eqns (5) and (7) into eqn (8), we get

$$\delta\pi = \{\delta a^*\}^T\{\mathbf{p}_B^{(1)}\}, \tag{9}$$

where $\mathbf{p}_B^{(1)}$ is the generalized interaction force between $R_1$ and $R_2$ and is given by

$$\{\mathbf{p}_B^{(1)}\} = [R]\{a\} + \{\mathbf{p}_B^{(0)}\} \tag{10}$$

and

$$[R] = \int_B [G^*_{r0}]^T [F_{r0}]\, d\gamma, \tag{11}$$

$$\{\mathbf{p}_B^{(0)}\} = \int_B [G^*_{r0}]^T \{\sigma^{(0)}_{r_g}\}\, d\gamma.$$

Substituting eqn (6) into eqn (1) and taking variation, we obtain

$$\begin{bmatrix} S_{II} & S_{IB}G_{xy} \\ G^{*T}_{xy}S^T_{IB} & G^{*T}_{xy}S_{BB}G_{xy} \end{bmatrix} \begin{Bmatrix} \mathbf{q}_{x_I} \\ a \end{Bmatrix} = \begin{Bmatrix} -S_{IB}\mathbf{q}^{(0)}_{x_g} \\ -G^{*T}_{xy}S_{BB}\mathbf{q}^{(0)}_{x_g} + \mathbf{p}^{(1)}_B \end{Bmatrix}, \tag{12}$$

where $\mathbf{q}^{(0)}_{x_g} = \{u^{(0)}_{x_j}, u^{(0)}_{y_{g_j}}\}^T$, and continuity of displacements and traction forces at boundary $B$ is imposed. It is seen from eqn (12) that the first equation can be written as

$$\{\mathbf{q}_{x_I}\} = [-S_{II}^{-1}S_{IB}G_{xy}a + S_{IB}\mathbf{q}^{(0)}_{x_g}]. \tag{13}$$

Substituting (10) and (13) into the second equation of eqn (12), we obtain

$$[G^{*T}_{xy}(S_{BB} - S^T_{IB}S_{II}^{-1}S_{IB})G_{xy} - R]\{a\} = -G^{*T}_{xy}(S_{BB} - S^T_{IB}S_{II}^{-1}S_{IB})\mathbf{q}^{(0)}_{x_g} + \mathbf{p}^{(0)}_B. \tag{14}$$

Once eqn (14) is solved for $\{a\}$, exterior and interior fields can be calculated from eqn (4) and eqn (13), respectively. In this paper results for the stress intensity factors obtained from the nodal displacements near the crack tip are discussed. The results for the surface displacements are presented elsewhere[29].

## 3. NUMERICAL RESULTS AND DISCUSSION

The displacements $\mathbf{q}_{x_I}$ at the nodal points within $B$ are computed by the method outlined above. The radius of the circle $B$ was chosen to be 1.6 times the half crack-length. Total number of equispaced nodes on $B$ was 48, and the number of nodes within $B$ was 308. Isoparametric finite elements similar to those discussed in [28] were used, namely, six-node triangular quarter-point singular elements near the crack-tips which were surrounded by a layer of seven-node transitional elements. Mostly four-point quadrilateral elements and some triangular elements were used in the rest of the domain $B$.

The stress intensity factors $K_I$ and $K_{II}$ are calculated from the crack opening displacement (COD) near a crack-tip by the relations

$$\begin{Bmatrix} K_I \\ K_{II} \end{Bmatrix} = \frac{\mu}{4(1-\nu)} \left(\frac{1}{L}\right)^{1/2} \begin{Bmatrix} \Delta_1 \\ \Delta_2 \end{Bmatrix}, \tag{15}$$

when

$$\Delta_1 = 4(v_6 - v_4) - (v_3 - v_2),$$
$$\Delta_2 = 4(u_6 - u_4) - (u_3 - u_2).$$

In the above equation $v_i$ and $u_i$ represent the jump in the displacement components $u_y$ and $u_x$, respectively at the $i$th node. The nodes 2, 3, 4 and 6 along with $L$ were defined in [28]. Here $\nu$ is the Poisson's ratio of the material.

In Figs 2(a) and (b) we show the comparison with the results presented in [5] for the case of an incident Rayleigh wave when $\alpha = 90°$. It is noted that labels on the vertical axes of Fig. 6 in [5] are to be interchanged. Agreement is found to be quite good in this case

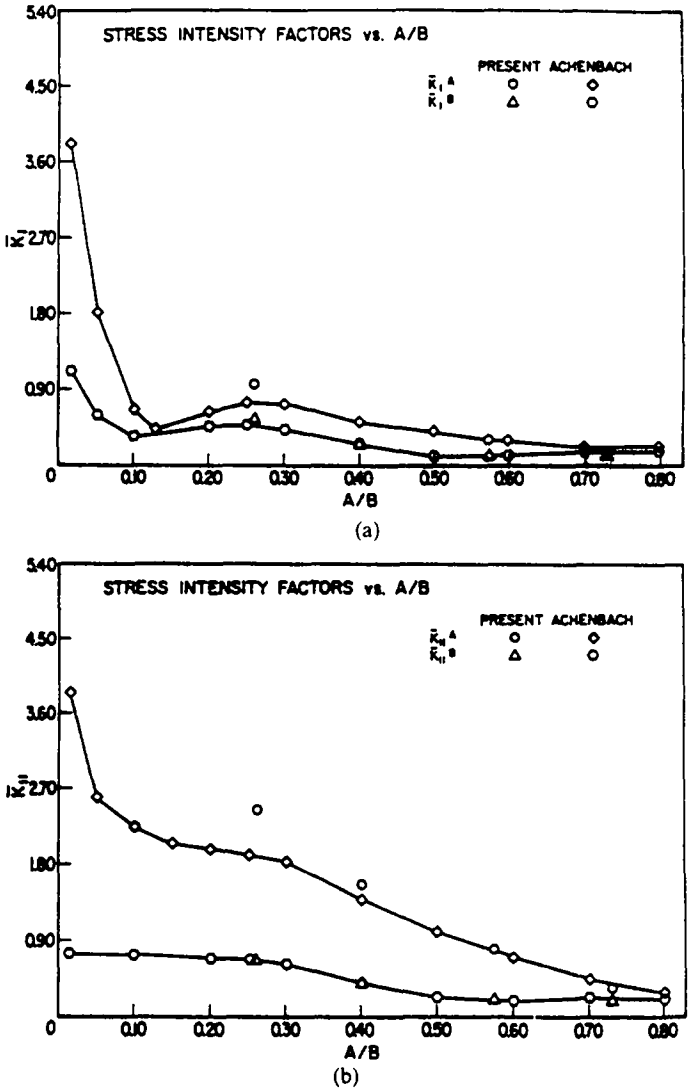


Fig. 2. Comparison of the mode 1 and mode 2 stress intensity factors with those of [5]. $\alpha = 90^{\circ}$. $A = H-L$, $B = H+L$.

except when the upper crack-tip comes very close to the surface. This is to be expected since as $A$ approaches the free surface the circular boundary $B$ comes very close to the surface, and the near-field expansions given by (4) become very slowly convergent. Figures 3(a) and (b) show the results for a horizontal ($\alpha = 0^{\circ}$) crack in comparison with those presented in

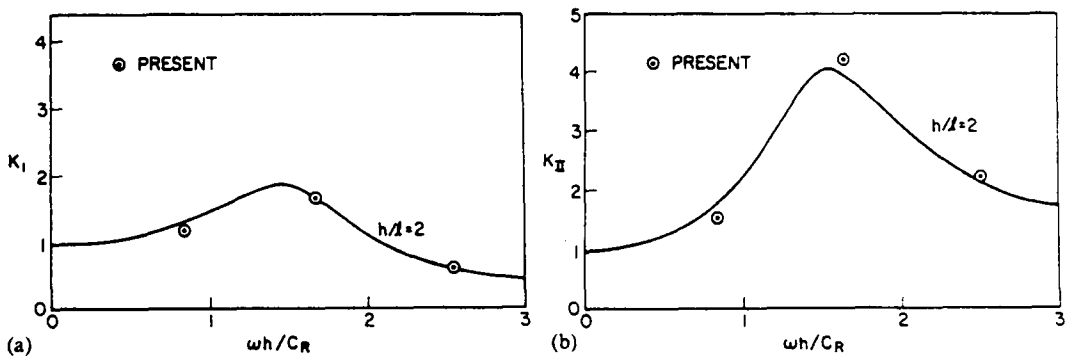


Fig. 3. Comparison of the mode 1 and mode 2 stress intensity factors for a horizontal crack with those of [7]. Here $K_I$ and $K_{II}$ are the ratios of the dynamic and static stress intensity factors.

[7]. The loading in this case is that given by either

$$\mathbf{q}_x^{(0)} = u_0 \, e^{ik_1(y-c_1 t)} \mathbf{e}_y \tag{16}$$

or

$$\mathbf{q}_x^{(0)} = v_0 \, e^{ik_2(y-c_2 t)} \mathbf{e}_x. \tag{17}$$

The agreement is again seen to be quite good.

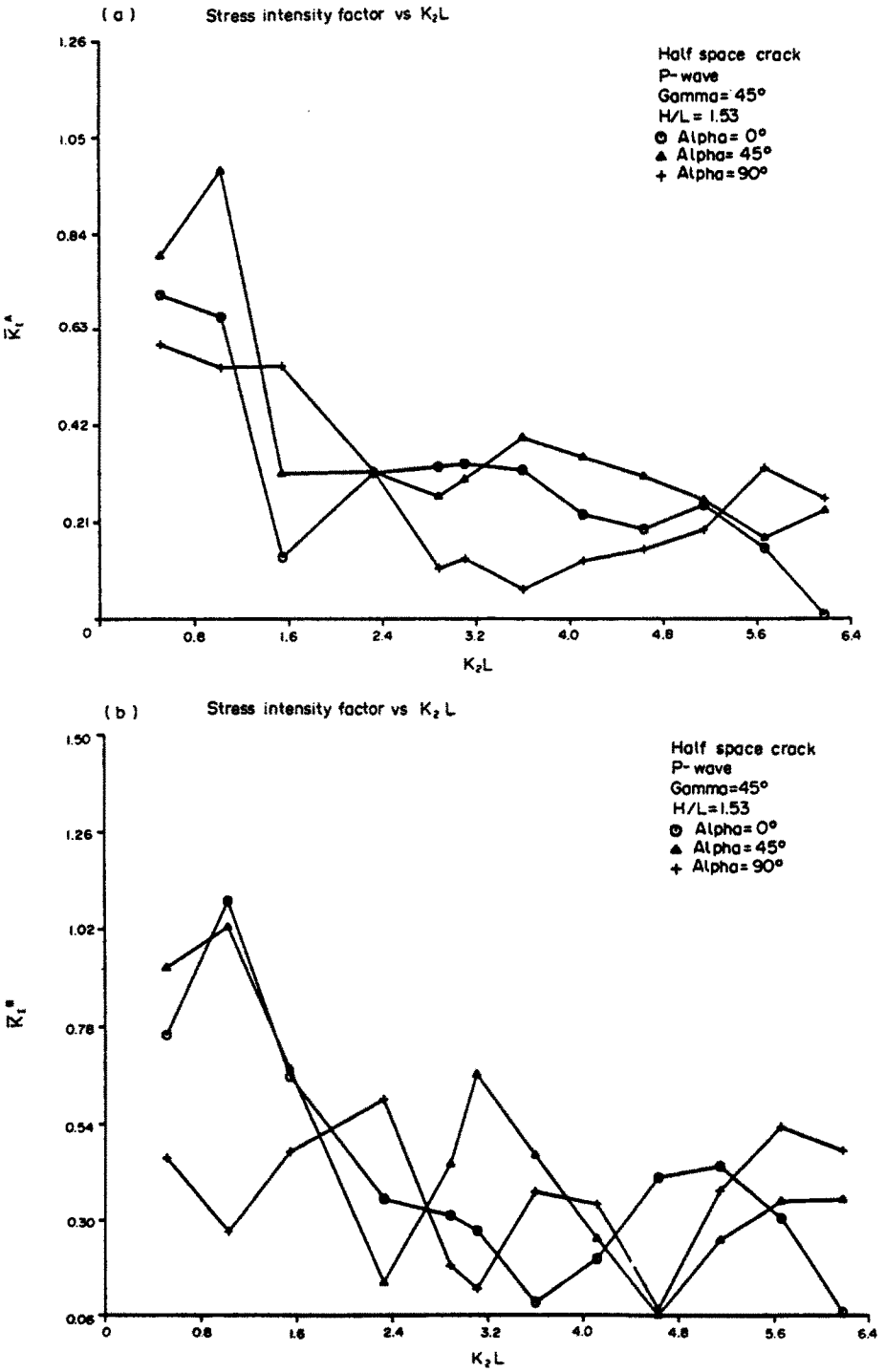


Fig. 4. Mode I stress intensity factors at the upper and lower crack tips for different crack orientation angles.

We now present the results for the normalized stress intensity factors for an inclined crack with $\alpha = 45°$ in comparison with those for the vertical ($\alpha = 90°$) and horizontal ($\alpha = 0°$) cracks. Figures 4–6 are for P and SV waves with the angle of inclination 45° to the negative $y$-axis. It is not surprising to note that for the SV wave 45°-inclined crack has the largest stress intensity factors. For P wave, on the other hand, this seems to be true at low

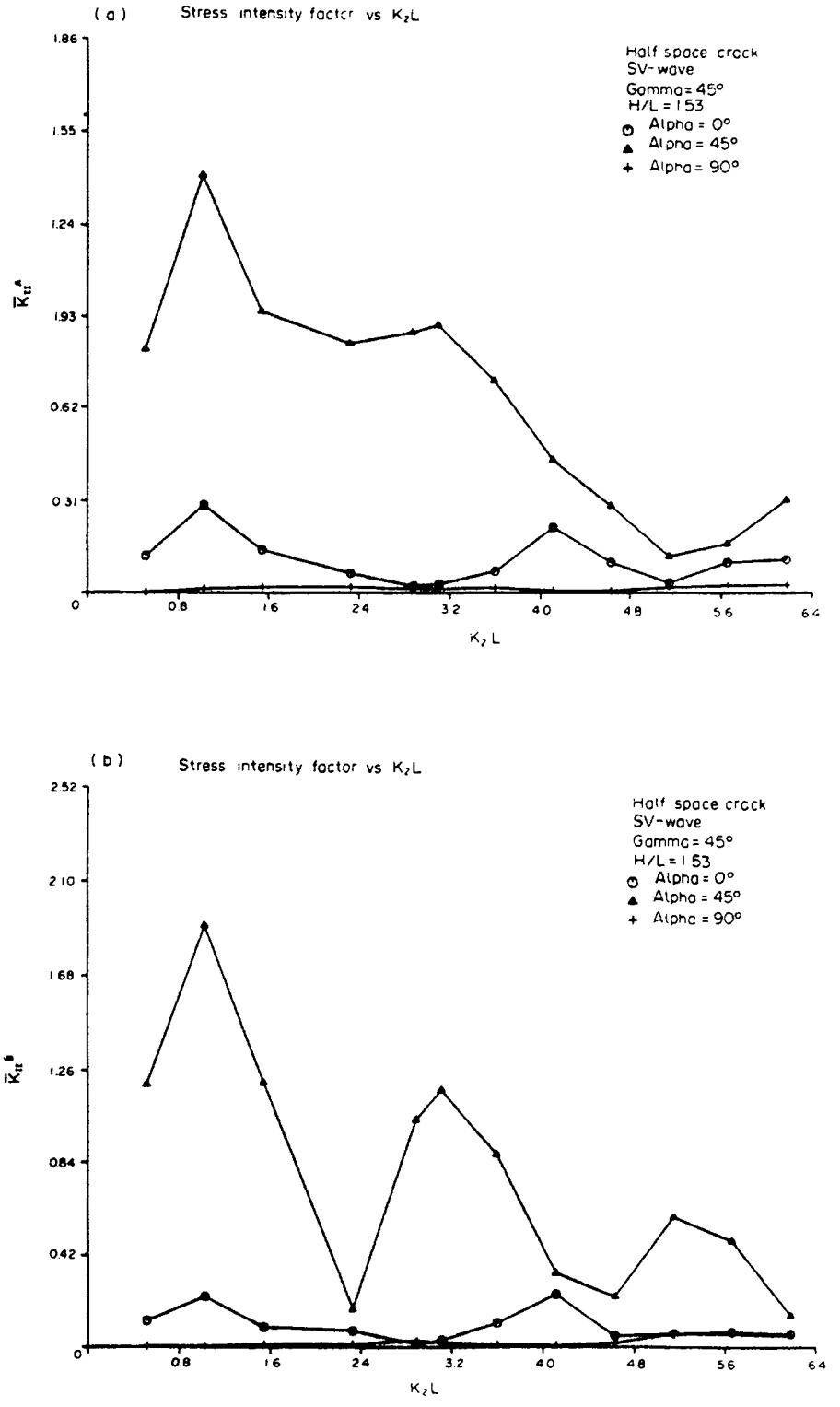


**Fig. 5. Mode 2 stress intensity factors at the upper and lower crack tips for different crack orientation angles.**

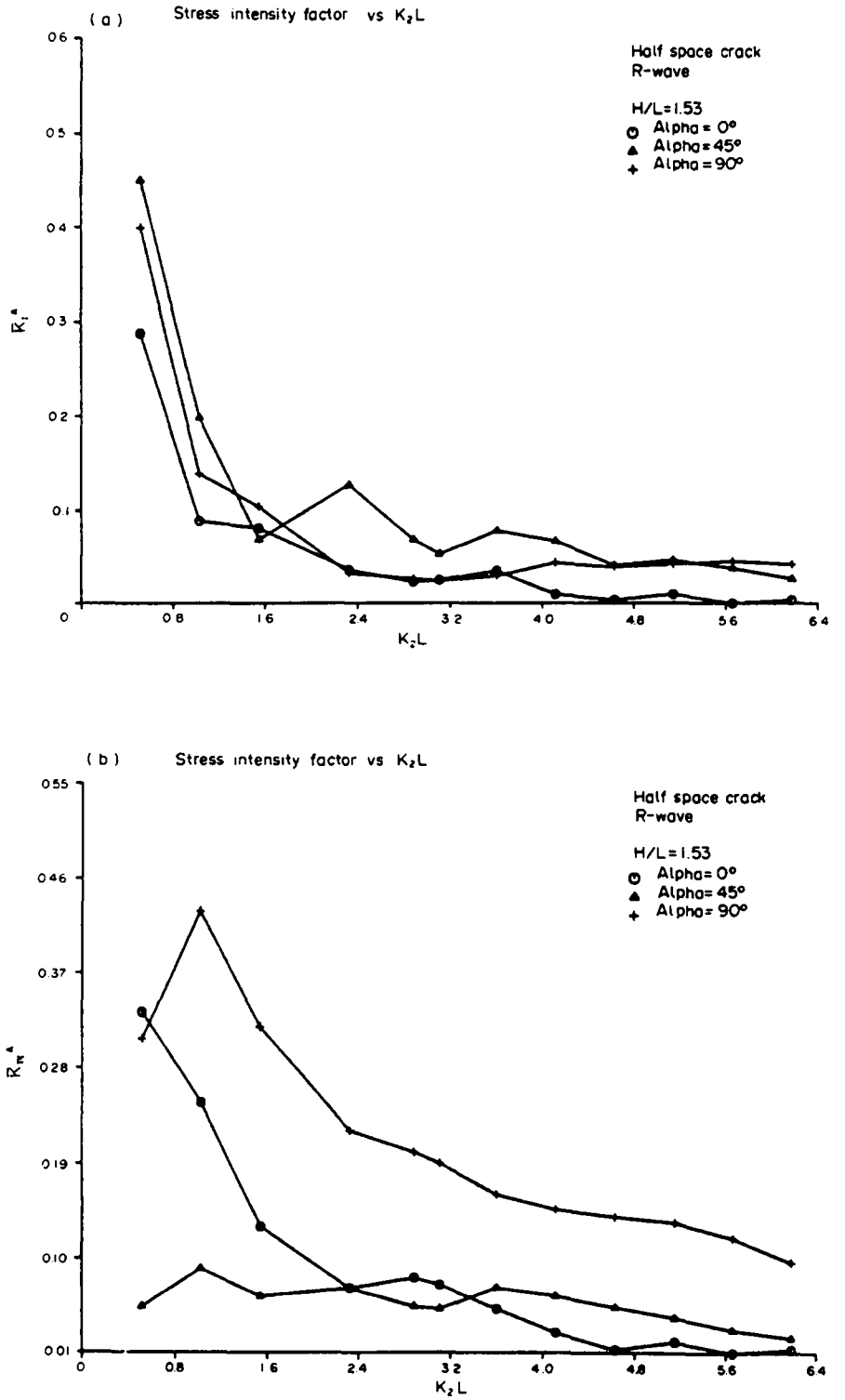


Fig. 6. Mode 1 and mode 2 stress intensity factors at the upper crack tip for Rayleigh wave incident on an inclined crack from the left.

frequencies but not at other frequencies. Results for Rayleigh wave are presented in Figs. 6(a) and (b).

Figures 7(a) and (b) show the results for a vertical crack at different depths for incident SV waves. Also shown on these figures are the results for a crack in an infinite medium. Even at large $H/L$ the results are found to be quite different from those in an infinite medium.

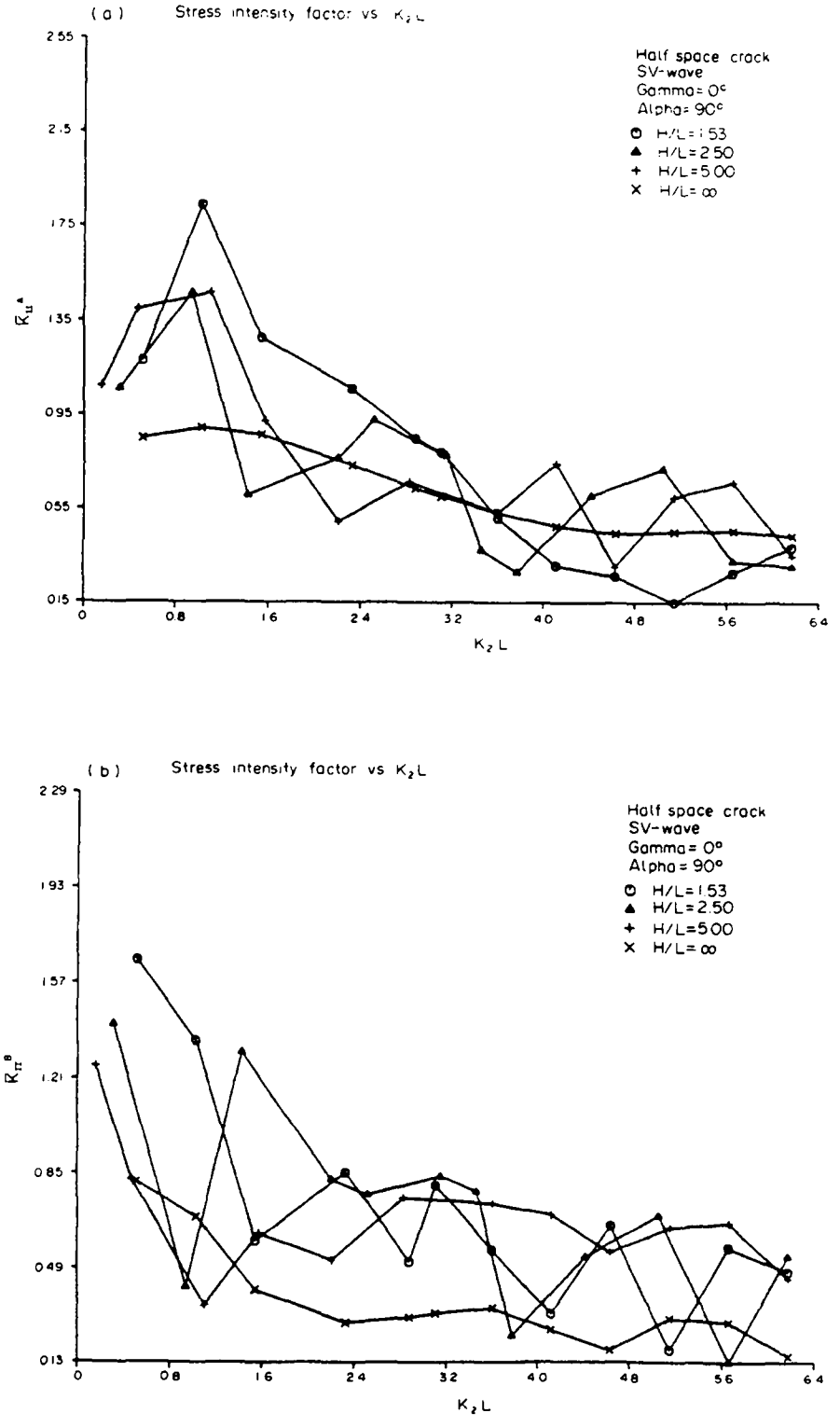


Fig. 7. Mode 2 stress intensity factors at the upper and lower crack tips of a vertical crack embedded at different depths for an incident SV wave.

Since cracks are not always straight we considered a crack with two branches (a Y crack). Some of these are presented when this is vertical [Fig. 1(b)]. Figures 8(a) and (b) show the stress intensity factors at the top branch tips ($B$ and $C$) in comparison to those at the top tip of a straight crack. For P-wave incidence, the mode $I$ stress intensity factor at the branch tips is found to be slightly lower than that at the top tip of a straight crack

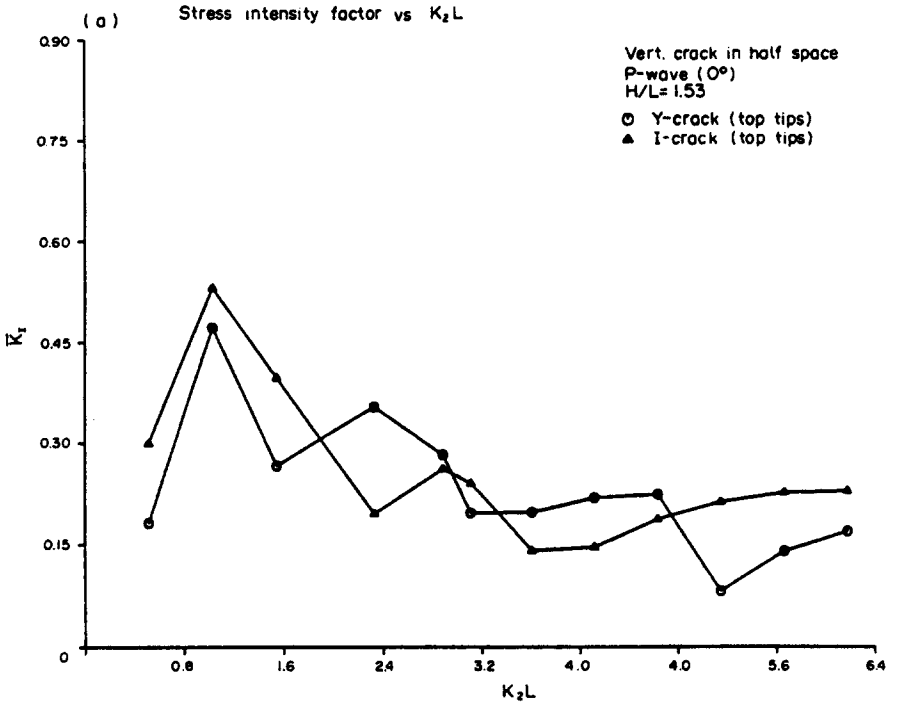


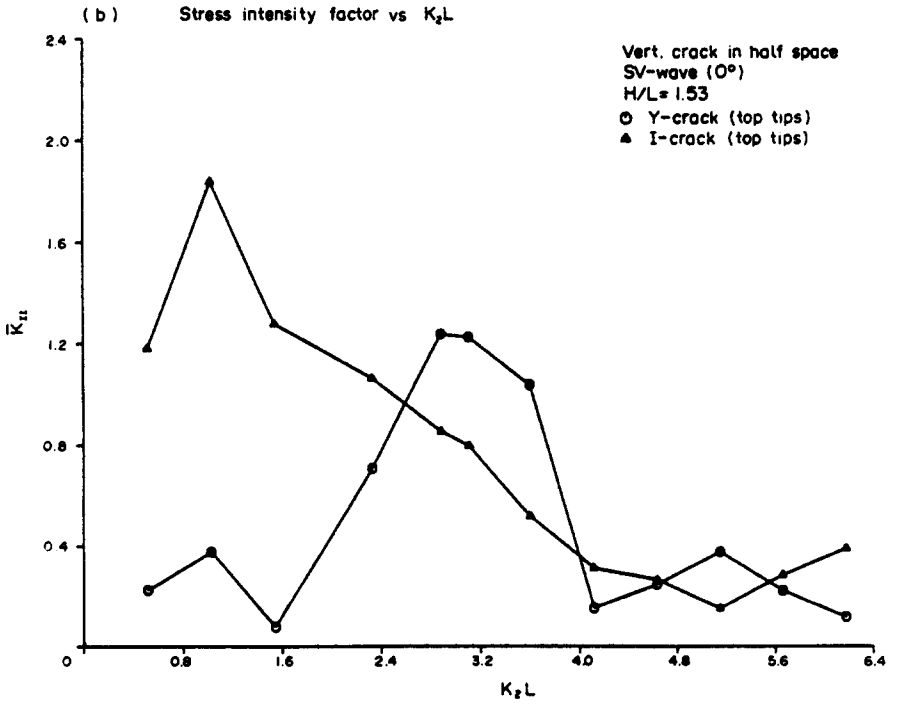


Fig. 8. Comparison of the stress intensity factors at the upper crack tips of vertical Y and straight cracks.

when the frequency is low. For SV wave the difference in the stress intensity factors in the two cases is seen to be much greater at low frequencies. Finally, in Figs. 9(a) and (b), we show the results for a Rayleigh wave. It is seen that the mode *I* stress intensity factor at the left branch tip is generally larger than that at the right one. The mode 2 stress intensity factor is found to behave in just the opposite manner.

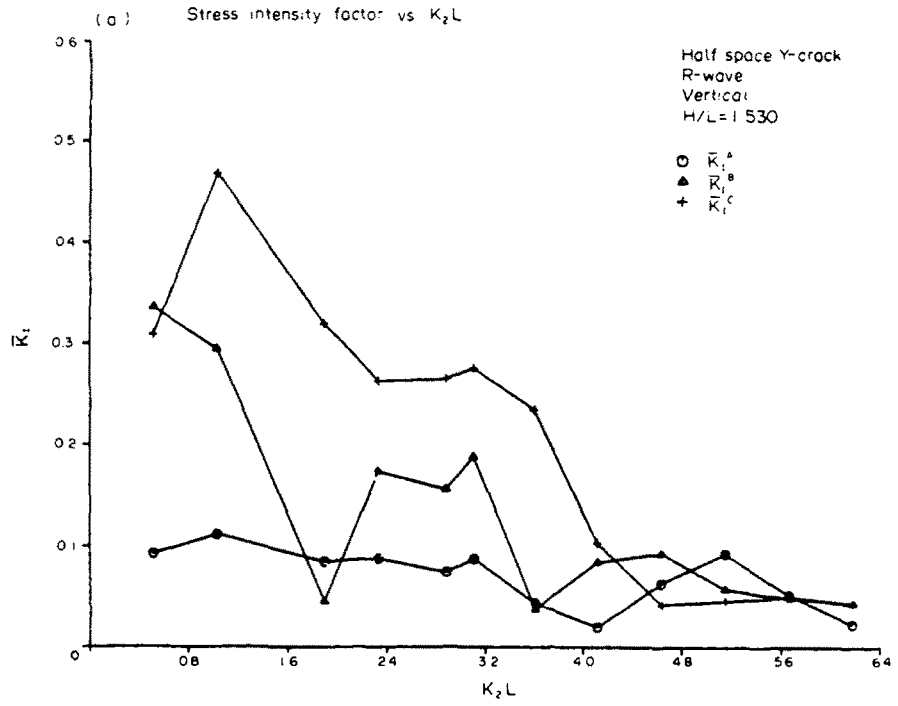


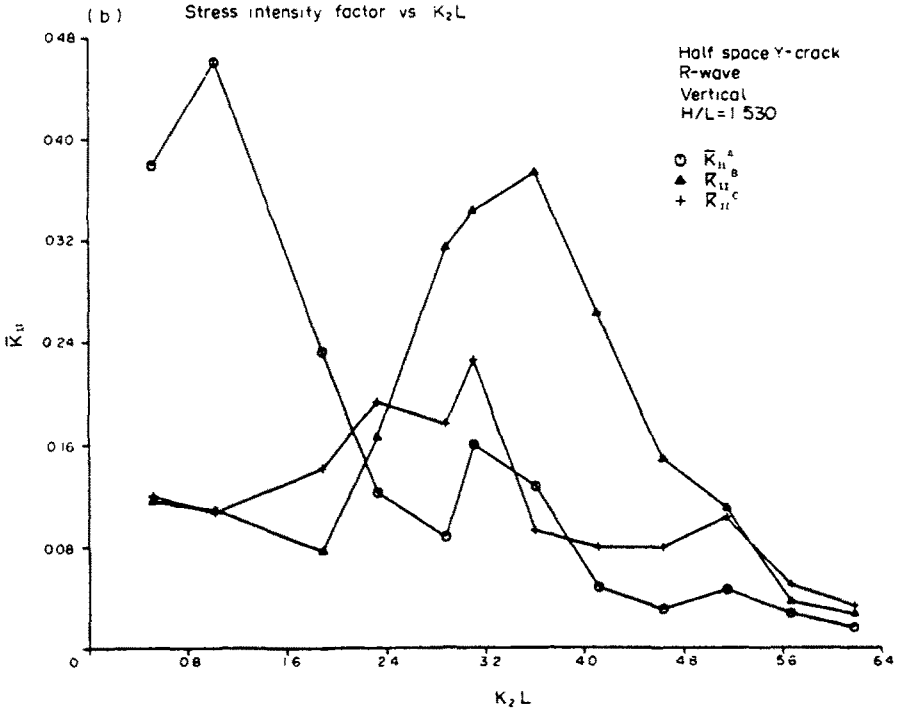


Fig. 9. Mode 1 and mode 2 stress intensity factors at the upper and lower crack tips of a Y crack for a Rayleigh wave incident from the left.

## 4. CONCLUSION

A combined finite element and analytical technique has been used to study the dynamic stress intensity factors at the tips of straight and branched (Y) cracks. Comparison of the results with other published ones are generally found to be good. It is found that the crack

tip stress intensity factors change significantly with depth and orientation of straight cracks. Also results for straight and branched cracks are quite different. It has been assumed here that the crack is not too close to the free surface, so that it can be enclosed by a circle centered at the crack center. However, this can be relaxed by using the integral expressions for the potential pairs $(\Phi_n^p, \psi_n^p)$ and $(\Phi_n^s, \psi_n^s)$ given in [27]. This work is in progress and will be reported later.

*Acknowledgement*—The work reported here was supported in part by grant A-7988 from the Natural Science and Engineering Research Council of Canada.

## REFERENCES

1. W. C. Luong, L. M. Keer and J. D. Achenbach, Elastodynamic stress intensity factors of a crack near an interface. *Int. J. Solids Structures* **11**, 919–925 (1975).
2. D. A. Mendelsohn, J. D. Achenbach and L. M. Keer, Scattering of elastic waves by a surface-breaking crack. *Wave Motion* **2**, 277–292 (1980).
3. J. D. Achenbach, L. M. Keer and D. A. Mendelsohn, Elastodynamic analysis of an edge crack. *J. Appl. Mech.* **47**, 551–556 (1980).
4. J. D. Achenbach and R. J. Brind, Elastodynamic stress–intensity factors for a crack near a free surface. *J. Appl. Mech* **48**, 539–542 (1981).
5. J. D. Achenbach and R. J. Brind, Scattering of surface waves by a sub-surface crack. *J. Sound Vibr.* **76**, 43–56 (1981).
6. R. J. Brind and J. D. Achenbach, Scattering of longitudinal and transverse waves by a sub-surface crack. *J. Sound Vibr.* **78**, 555–563 (1981).
7. L. M. Keer, W. Lin and J. D. Achenbach, Resonance effects for a crack near a free surface. *J. Appl. Mech.* **51**, 65–70 (1984).
8. J. D. Achenbach, W. Lin and L. M. Keer, Surface waves due to scattering by a near-surface parallel crack. *IEEE Trans. Sonics Ultrasonics* **SU-30**, 270–276 (1983).
9. W. Lin, L. M. Keer and J. D. Achenbach, Dynamic stress intensity factors for an inclined subsurface crack. *J. Appl. Mech.* **51**, 773–779 (1984).
10. J. D. Achenbach and A. K. Gautesen, A ray theory for elasto-dynamic stress-intensity factors. *J. Appl. Mech.* **45**, 123–129 (1978).
11. A. K. Gautesen, J. D. Achenbach and H. McMaken, Surface wave rays in elastodynamic diffraction by cracks. *J. Acoust. Soc. Am.* **63**, 1824–1831 (1978).
12. J. D. Achenbach, A. K. Gautesen and D. A. Mendelsohn, Ray analysis of surface-wave interaction with an edge crack. *IEEE Trans. Sonics Ultrasonics* **SU-27**, 124–129 (1980).
13. J. D. Achenbach and A. N. Norris, Interference of corner reflected and edge diffracted signals for a surface-breaking crack. *J. Acoust. Soc. Am.* **70**, 165–171 (1981).
14. J. D. Achenbach, A. K. Gautesen and H. McMaken, *Ray Methods for Waves in Elastic Solids—with Applications to Scattering by Cracks*. Pitman, London (1982).
15. W. M. Visscher, Elastic wave scattering by a surface-breaking or sub-surface planar crack. II. Three-dimensional geometry. *J. Appl. Phys.* **57**, 1538–1550 (1985).
16. S. F. Stone, M. L. Ghosh and A. K. Mal, Diffraction of antiplane shear waves by an edge crack. *J. Appl. Mech.* **47**, 359–362 (1980).
17. S. K. Datta, Diffraction of SH-waves by an edge crack. *J. Appl. Mech.* **46**, 101–106 (1979).
18. S. K. Datta, A. H. Shah and C. M. Fortunko, Diffraction of medium and long wavelength horizontally polarized shear waves by edge cracks. *J. Appl. Phys.* **53**, 2895–2903 (1982).
19. S. K. Datta and A. H. Shah, Diffraction of horizontally polarized shear waves. In *Numerical Methods in Engineering* (Edited by P. Lascaux), Vol 2, pp. 447–457. Pluralis, Paris (1983).
20. Z. Abduljabbar, S. K. Datta and A. H. Shah, Diffraction of horizontally polarized shear waves by normal edge cracks in a plate. *J. Appl. Phys.* **54**, 461–472 (1983).
21. Z. Abduljabbar and S. K. Datta, Diffraction of horizontally polarized shear waves by cracks in a plate. International Conference on Numerical Methods for Transient and Coupled Problems, July 9–13, Venice, Italy (1983).
22. Z. Abduljabbar, Diffraction of horizontally polarized shear waves in a plate. Ph.D. Thesis, University of Colorado, Boulder (1983).
23. S. K. Datta, A. H. Shah and K. C. Wong, Dynamic stresses and displacements in buried pipe. *J. Engng Mech. ASCE* **110**, 1451–1466 (1984).
24. A. H. Shah, K. C. Wong and S. K. Datta, Single and multiple scattering of elastic waves in two dimensions. *J. Acoust. Soc. Am.* **74**, 1033–1043 (1983).
25. K. C. Wong, A. H. Shah and S. K. Datta, Diffraction of elastic waves in a half-space. II. Analytical and numerical solutions. *Bull. Seism. Soc. Am.* **75**, 69–92 (1985).
26. S. K. Datta and N. El-Akily, Diffraction of elastic waves in a half-space. I: Integral representation and matched asymptotic expansions. In *Modern Problems in Elastic Wave Propagation* (Edited by J. Miklowitz and J. D. Achenbach), pp. 197–218. Wiley, New York (1978).
27. S. K. Datta and N. El-Akily, Diffraction of elastic waves by cylindrical cavity in a half-space. *J. Acoust. Soc. Am.* **64**, 1692–1699 (1978).
28. S. K. Datta and A. H. Shah, Scattering of SH waves by embedded cavities. *Wave Motion* **4**, 265–283 (1982).
29. A. H. Shah, K. C. Wong and S. K. Datta, Surface displacements due to elastic wave scattering by planar and non-planar cracks. *Wave Motion* **7**, 319–333 (1985).